

¹ **1. Preliminary analyses**

² Based on the WRF datasets referred by Daniel, I have looked into the relevant changes of
³ precipitation (focused on winter season) from the past (year 1991-2000) to the future (presumably
⁴ year 2091-2100). Here are some initial investigation (mainly in the qualitative aspect) with
⁵ supported rough plots attached.

⁶

⁷ 1) How well does WRF reproduce the historical mean precipitation compared to observations
⁸ (here, only show PRISM)?

⁹ As shown in the plot (see Figure 1), WRF performed quite good compared to PRISM, although
¹⁰ there are notable biases over the mountain peaks as the grid resolution increased to 3 km.

¹¹

¹² 2) With the intensified thermodynamic forcing, how precipitation is projected to be changed
¹³ over California? How about the orographic precipitation over the Sierra Nevada (SN)?

¹⁴ Overall, as climate keeps warming prescribed by RCP 8.5, the ensemble mean Pr from the five
¹⁵ selected GCMs is projected to increase moderately mainly over the wet area (i.e. the North coast
¹⁶ and mountainous area) (please see Figure 2 and Figure 3). Specifically, within the five models,
¹⁷ three show increasing trend with diverse magnitude; The other two show either minor changes or
¹⁸ opposite trend over SN. The overall changing trends from the dynamically downscaled results of
¹⁹ WRF are consistent with five GCMs' output except for model inmcm4 when referred to Figure 2
²⁰ in Daniels paper about the snowpack (Walton et al. 2016).

²¹

22 3) How about the changes of different precipitation events (here, simply dividing into the low-
23 rainy, the high-rainy and the extreme)? To what extent, the changes of these different rainy events
24 contribute to the overall changes of Pr?

25 When looking at Figure 4, it can be found that low-rainy events act as a negative factor to
26 the changes of precipitation in the future from the ensemble mean result over eastern area of the
27 Central Valley and windward of Sierra Nevada. Again, there are inconsistent behaviors within
28 the five models, especially when we compare the GFDL model and the MPI model to the other
29 three remaining models. Particularly, in the GFDL model, there are disorganized signals of the
30 changes, which might be related with the downscaling of the regional wind circulation pattern with
31 unresolved processes.

32 The high-rainy days have increased and contributed mainly to the mean precipitation increase
33 over the coastal area, the Central Valley, southern part and the relatively low-level of the moun-
34 tainous regions (see Figure 5). However, over the high-level mountainous area, the precipitation
35 changes mainly result from extreme events (see Figure 6).

36 Further, the frequency distribution is roughly conveyed in the Figure 7, showing the frequency
37 of the low-rainy, the high-rainy and the extreme over the historical period (i.e. year 1991-2000)
38 and their corresponding contributions to the total rainy amount. This further supports that the
39 precipitation over both dry and wet area over California will tend to be more extreme with the
40 distribution shifts with higher upper tail.

41
42 4) As the temperature increases in the future, whether the specific humidity will enlarge followed
43 by the Clausius-Clapeyron (C-C) relationship?

44 The relative changes of the specific humidity and its relationship to the temperature are given in
45 Figure 8 and 9. Overall the intensity of the specific humidity (Q2) changes is higher over the area

⁴⁶ where the temperature increases more. Specifically, the proportional changes of the Q2 contrast to
⁴⁷ the increases of T2 are higher than 7% over most regions reaching higher than 10% over the area
⁴⁸ warms most.

⁴⁹ 5) How the frequency of different rainy events is predicted to be changed?

⁵⁰ First, we look at the relative changes of total rainy days averaged during wet season. The result
⁵¹ shows a relative minor changes of rainy days except the lee side of Sierra Nevada (see Figure
⁵² 10). This pattern is even more obvious for low-rainy days as Figure 11 shown. In Figure 11,
⁵³ the outmost domain is displayed with the middle domain to see how the dynamical downscaling
⁵⁴ works. It seems that the higher resolution at 9km has more local features and tends to have less
⁵⁵ low-rainy days with finer topography, although the overall changes of low-rainy days are slight.

⁵⁶ For the heavy-rain events (see Figure 12 and Figure 13), the frequency has increased notable
⁵⁷ over both sides of SN, especial over the dry Central Valley and the lee side, but decreased over the
⁵⁸ mountain peaks.

⁵⁹ 6) How the frequency distribution of daily Pr changes over California from past to future?

⁶⁰ First, the 95th quantile (P95) of daily Pr at each grid point has been given here (see Figure
⁶¹ 14) to show a general picture that whether the upper tail of the Pr distribution has shifted and
⁶² how. Consistent with previous analyses, there are obvious increases of the P95 for three members
⁶³ (CNRM, INMCM, IPSL) and barely changes for the other two models (GFDL, MPI).

⁶⁴ To account for the diverse hydro-climate features over different regions of California (CA), the
⁶⁵ whole CA has been divided into five zones followed by Huang et al. (2016) (see wrf_domains.pdf
⁶⁶ in the folder). From the PDF plot (see Figure 15), it can be seen that in the end-century, overall,
⁶⁷ precipitation is projected to be more extreme over all the regions. Again, discrepancy exists within
⁶⁸ different model members as aforementioned.

69 7) The role of large-scale water vapor transport in regulating the heavy-rainy events over Cali-
70 fornia

71 The integrated water vapor transport (IVT) of the maximum one day Pr (averaged over whole
72 CA) is examined for each simulation to see the track of the water vapor influx during the most
73 heaviest rainy day over CA (see Figure 16). Along with the IVT, the near-surface wind pattern and
74 resulted Pr are also given in Figure 17, correlating the higher Pr for the future simulations with the
75 increased IVT in the form of atmospheric rivers (ARs) with the warming effect.

76 Statistically, the average IVT when the mean Pr over whole CA exceeds the P95 is given in
77 Figure 18. The P95 value is 14.2 mm/day (averaged over CA), and the number of days with Pr
78 being above P95 are 76, 130, 68, 110, 141 and 96 for hist and other five future simulations. This
79 might give us a general idea of both the thermodynamic (in the aspect of IVT) and dynamic (in
80 the aspect of wind circulation) effects for the future changes of heavy-rainy events.

81 As above mentioned, the IVT has notable increased with the warming effect, however, the wind
82 pattern shows diverse changes within different models. Specifically, even the heavy-rainy days
83 have increased largely (30%-85%) within the models (INMCM, IPSL and MPI), the changes of
84 wind patterns tend to play a negative effect with weaken westerly wind. The negative dynamic
85 effect for ARs has also been found by Gao et al. (2015) over western U.S. based on CMIP5 output.

86 For the GFDL model, the IVT has largely increased even with strengthen wind pattern, however,
87 the heavy-rainy days surprisingly show a minor decrease (10%). These changes still hold when
88 using P85 to account for more heavy-rainy events. For reference, the P85 value is 6.9 mm/day,
89 and the number of days with Pr being above P85 are 226, 278, 206, 255, 279 and 229 for hist and
90 other five future simulations.

91 **2. Discussions and further directions**

- 92 a) The possible reasons that affect the contradictory changes of precipitation within different
93 models.
94 b) sub-daily Pr dataset
95 c) hybrid dynamical downscaling
96 d) The relative change of T vertically over the Sierra Nevada, the condensation rate or cloud
97 liquid water

98 **check the microphysics in WRF, and how the parameters change the orographic precipitation
99 notes:

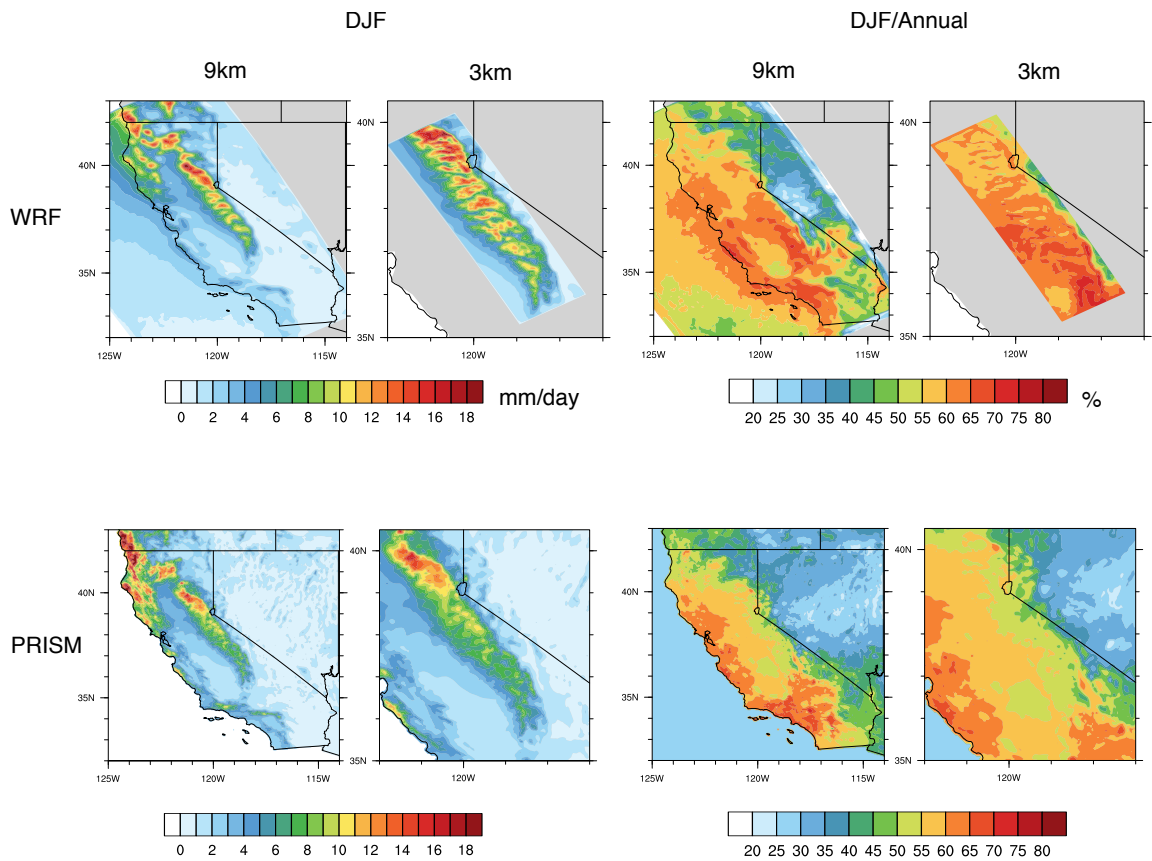
100 i) Alex: The lee side shows such a large percentage increase. This appears to be coming from the
101 low rainy days, but since precipitation is low there even during large events, this effect may actually
102 be associated with heavy precipitation events in California. This effect seems to be consistent with
103 Stiller and Roe. It would be very interesting to see whether in fact it is.

104 **References**

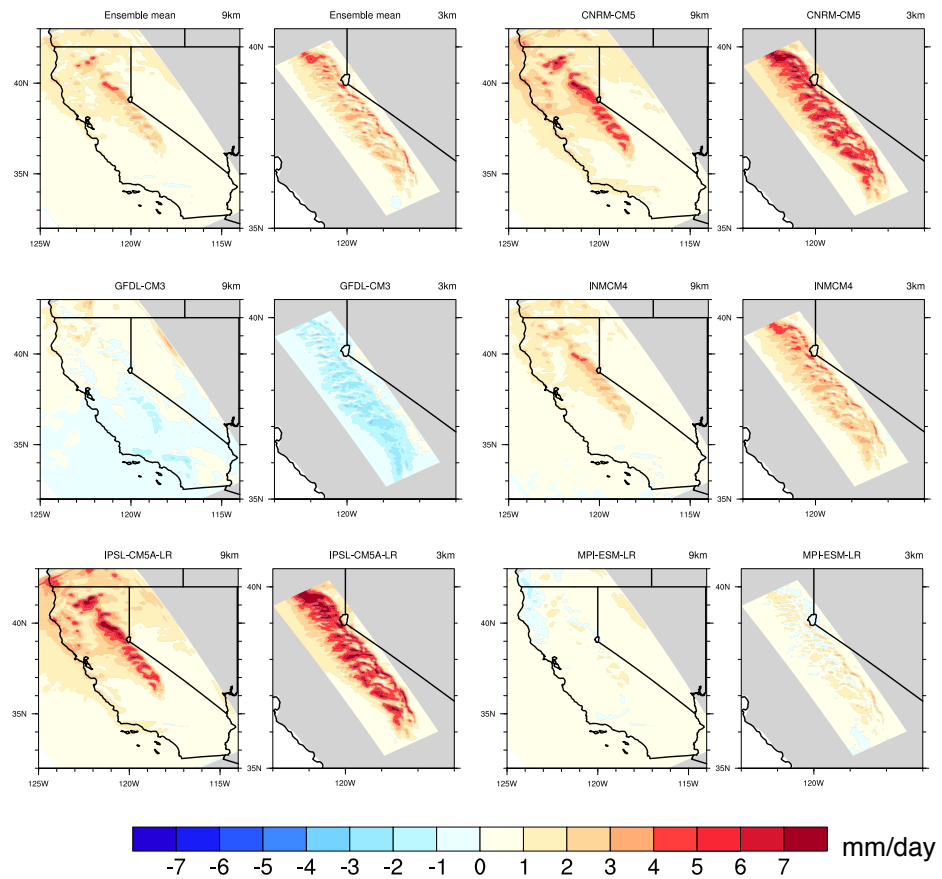
- 105 Gao, Y., J. Lu, L. R. Leung, Q. Yang, S. Hagos, and Y. Qian, 2015: Dynamical and thermodynamical
106 modulations on future changes of landfalling atmospheric rivers over western north america.
107 *Geophysical Research Letters*, **42** (17), 7179–7186.
- 108 Huang, X., A. M. Rhoades, P. A. Ullrich, and C. M. Zarzycki, 2016: An evaluation of the vari-
109 able resolution-cesm for modeling california's climate. *Journal of Advances in Modeling Earth*
110 *Systems*.
- 111 Walton, D. B., A. Hall, N. Berg, M. Schwartz, and F. Sun, 2016: Incorporating snow albedo
112 feedback into downscaled temperature and snow cover projections for californias sierra nevada.

114 LIST OF FIGURES

115	Fig. 1. The mean DJF precipitation (Pr) and its corresponding contribution to the annual Pr for WRF (9km and 3km) and PRISM, over the historical time period (year 1991-2000).	8
117	Fig. 2. The changes of mean DJF Pr from the past to future simulated by WRF at 9km and 3km from the five modes and model ensemble mean.	9
119	Fig. 3. Similar as Figure 2, but for the relative change in percentage.	10
120	Fig. 4. The relative contribution to the total precipitation changes resulted from the changes of low-rainy days ($Pr \leq 10\text{mm/day}$).	11
122	Fig. 5. Similar as Figure 4 but for the high-rainy days ($10\text{mm} < Pr \leq 60\text{mm/day}$).	12
123	Fig. 6. Similar as Figure 4 but for the precipitation extremes ($Pr > 60\text{mm/day}$).	13
124	Fig. 7. The frequency of the low-rainy, the high-rainy and the extreme over historical period (i.e. year 1991-2000) and their corresponding contributions to the total rainy amount.	14
126	Fig. 8. The relative changes of the specific humidity compared to historical period.	15
127	Fig. 9. The relative changes of the 2m specific humidity contrasted to the changes of 2m temperature.	16
129	Fig. 10. The relative changes of the rainy days during wet season (NDJFM) from past to future.	17
130	Fig. 11. Similar as Figure 10, but for low-rainy days.	18
131	Fig. 12. Similar as Figure 10, but for heavy-rainy days.	19
132	Fig. 13. Similar as Figure 10, but for extremes.	20
133	Fig. 14. The 95th quantile (P95) of daily Pr at each grid point for hist and future at 9 km.	21
134	Fig. 15. The frequency distribution of daily Pr ($>1\text{mm/day}$) based on all the grid points within different climate divisions for hist and future at 9 km. Note: (a) California, (b) Central Valley, (c) Mountain region, (d) Desert area, (e) North coast, (f) South coast.	22
137	Fig. 16. The integrated water vapor transport (IVT) of the maximum 1 day Pr during the simulation periods for hist and future at 27 km.	23
139	Fig. 17. The near-surface wind pattern (at 10 m, unit: m/s) and Pr of the maximum 1 day Pr event for hist and future at 9 km.	24
141	Fig. 18. The average IVT and mean wind pattern as the mean Pr over CA exceeds the P95 value for hist and future at 27 km. Note: Here, the wind patterns for future simulations are the difference between specific future simulation and historical result.	25
144	Fig. 19. Similar as Figure 18, but for the case when Pr exceeds the P85 value.	26



145 FIG. 1. The mean DJF precipitation (Pr) and its corresponding contribution to the annual Pr for WRF (9km
 146 and 3km) and PRISM, over the historical time period (year 1991-2000).



147 FIG. 2. The changes of mean DJF Pr from the past to future simulated by WRF at 9km and 3km from the five
148 modes and model ensemble mean.

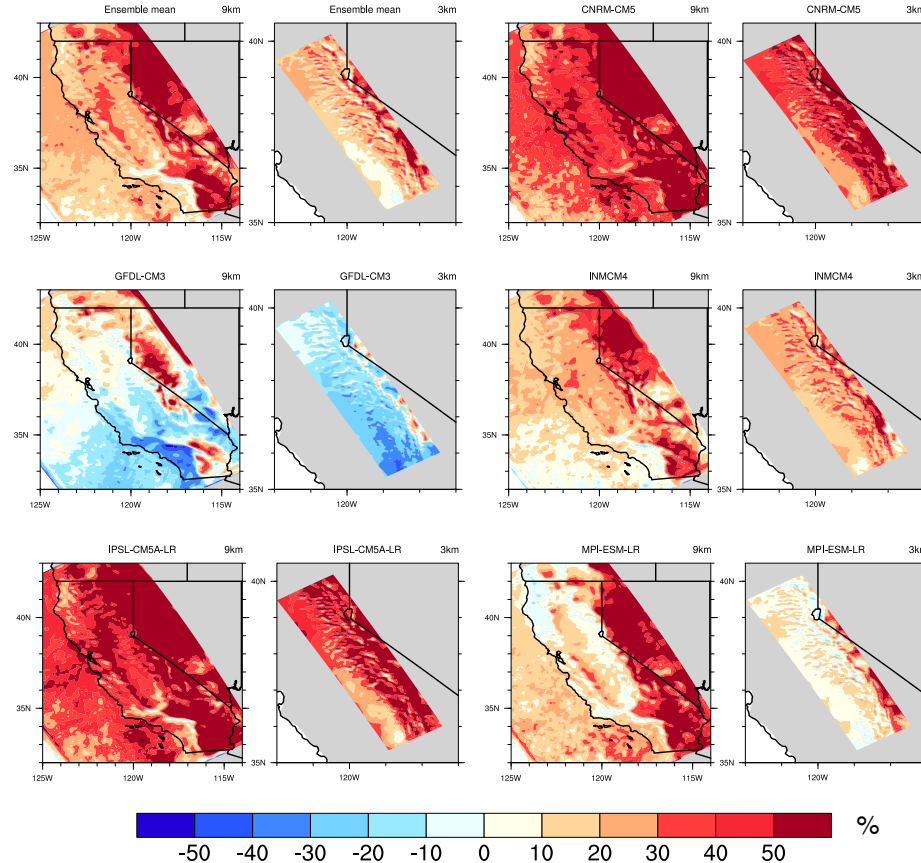
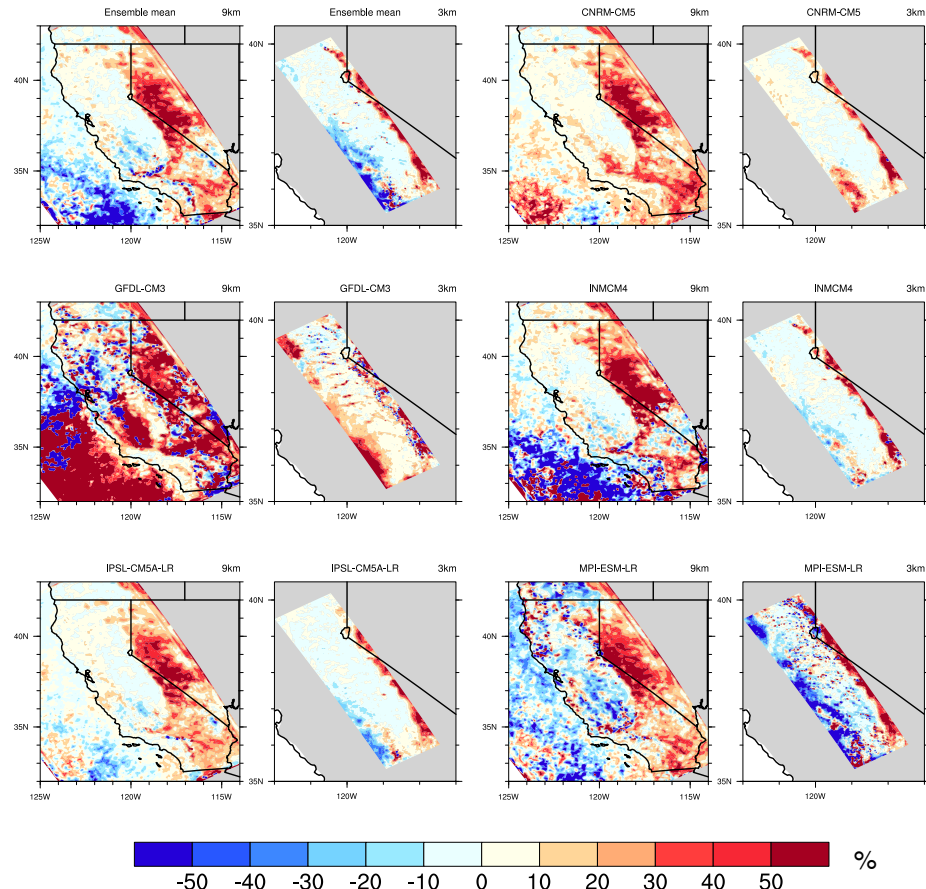


FIG. 3. Similar as Figure 2, but for the relative change in percentage.



149 FIG. 4. The relative contribution to the total precipitation changes resulted from the changes of low-rainy days
 150 ($\text{Pr} \leq 10\text{mm/day}$).

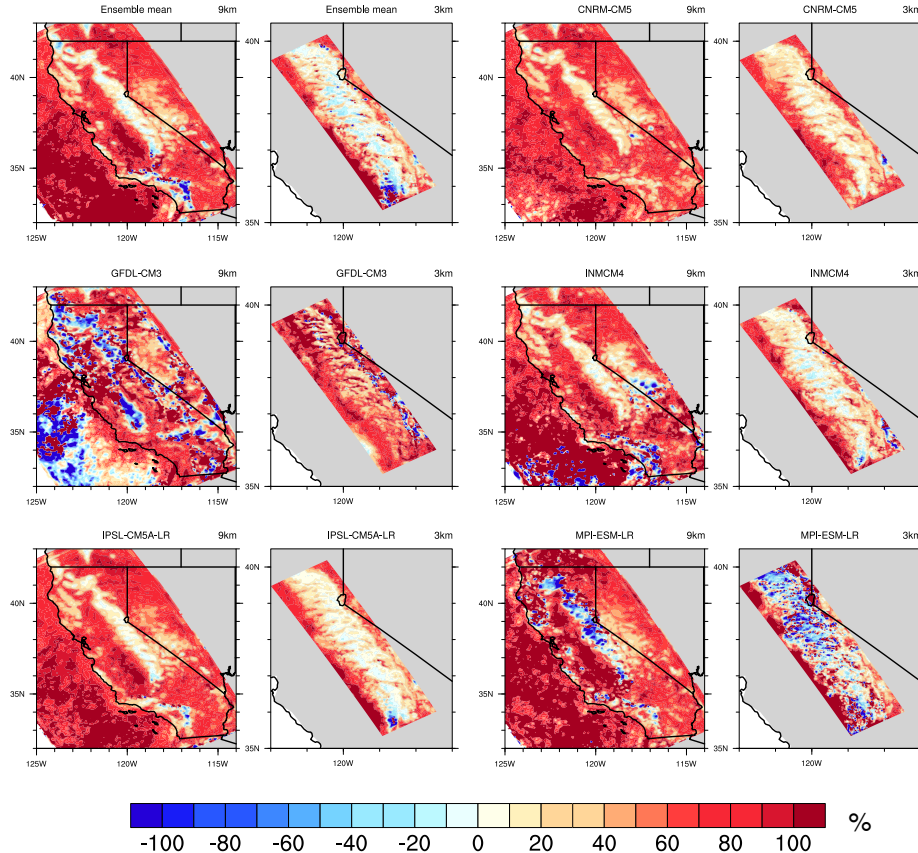


FIG. 5. Similar as Figure 4 but for the high-rainy days ($10\text{mm} < \text{Pr} \leq 60\text{mm/day}$).

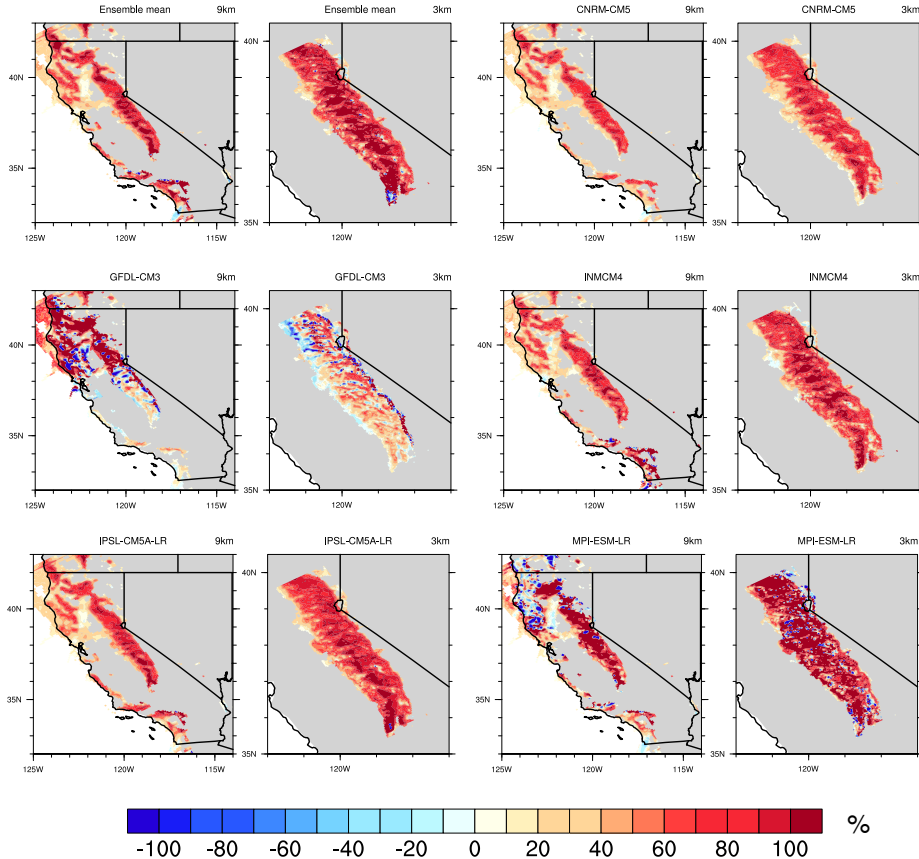
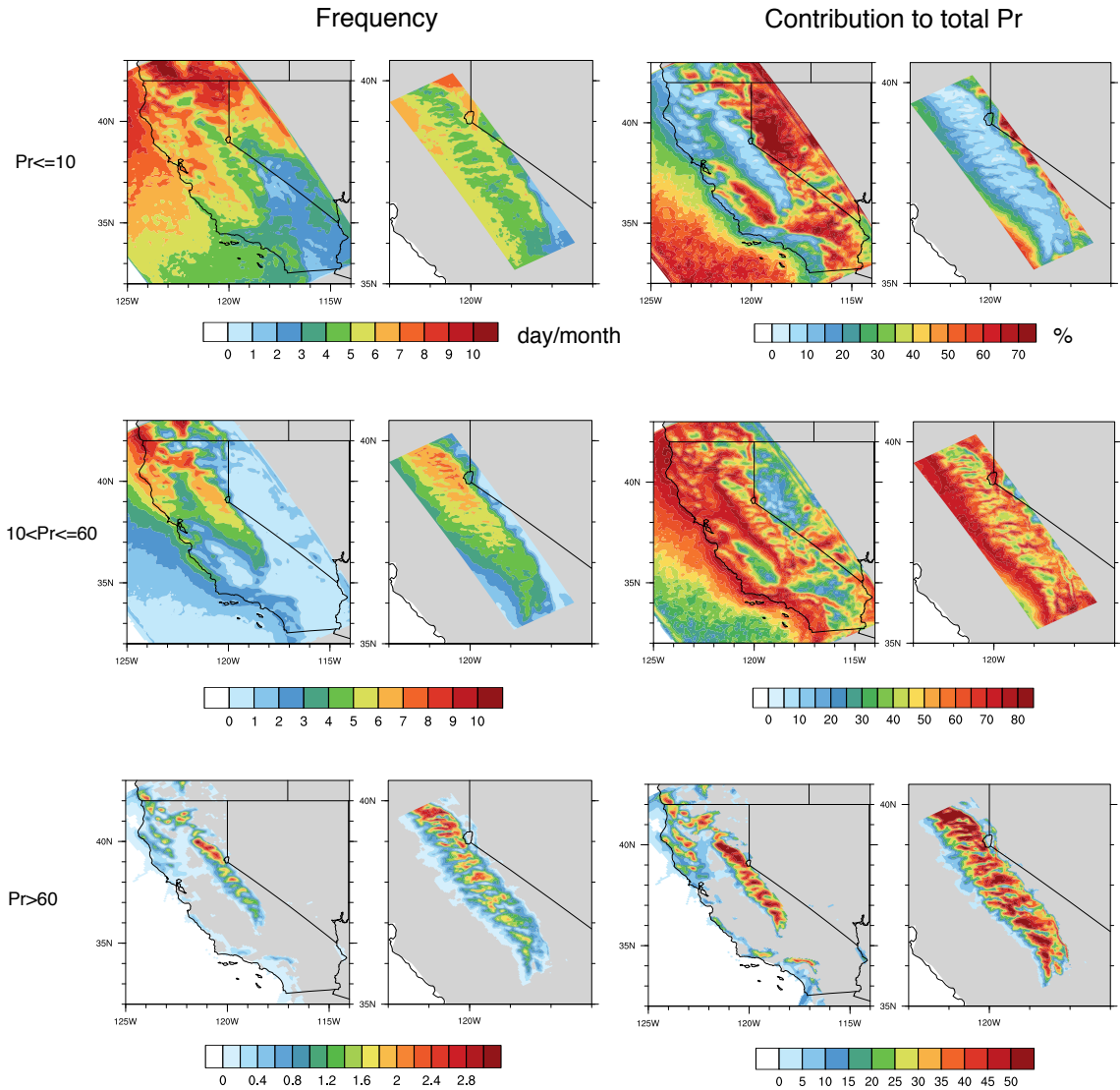


FIG. 6. Similar as Figure 4 but for the precipitation extremes ($\text{Pr} > 60\text{mm/day}$).



151 FIG. 7. The frequency of the low-rainy, the high-rainy and the extreme over historical period (i.e. year
 152 1991-2000) and their corresponding contributions to the total rainy amount.

2m Specific Humidity

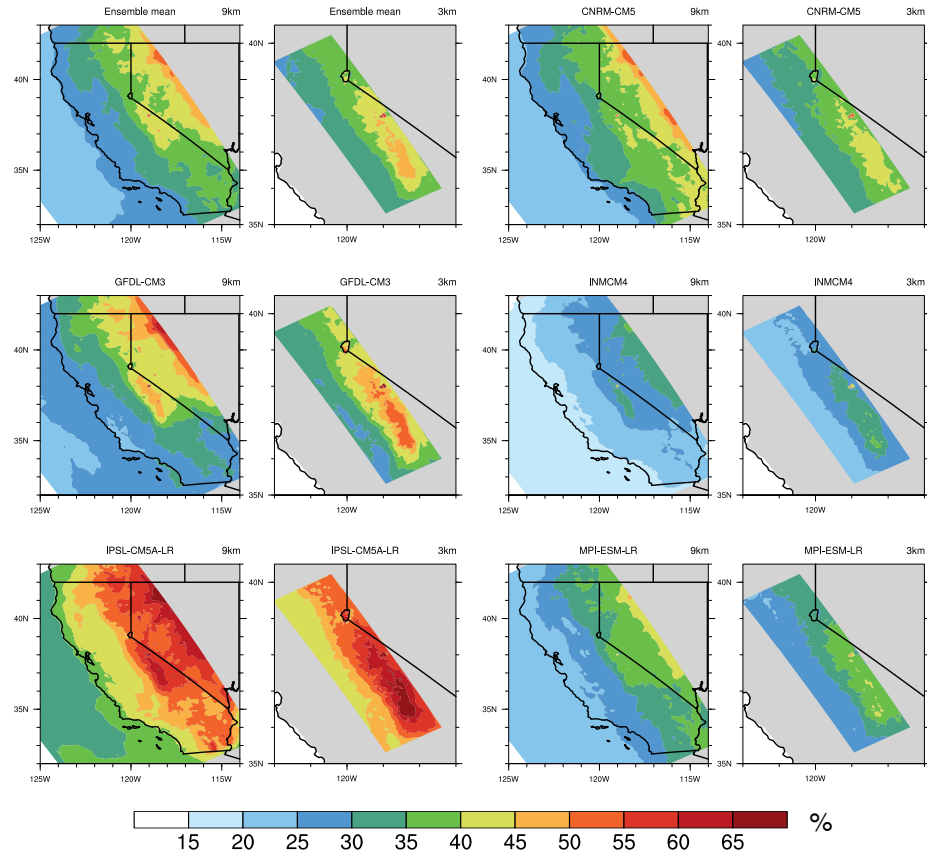


FIG. 8. The relative changes of the specific humidity compared to historical period.

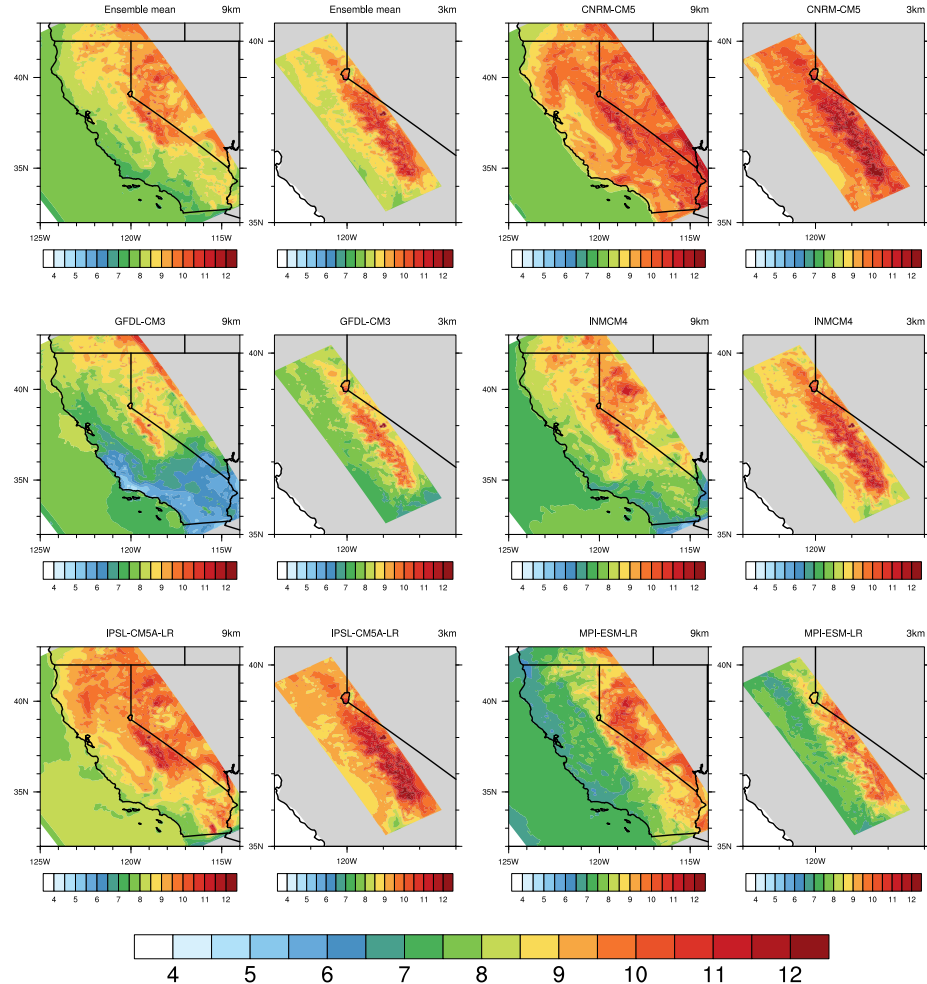


FIG. 9. The relative changes of the 2m specific humidity contrasted to the changes of 2m temperature.

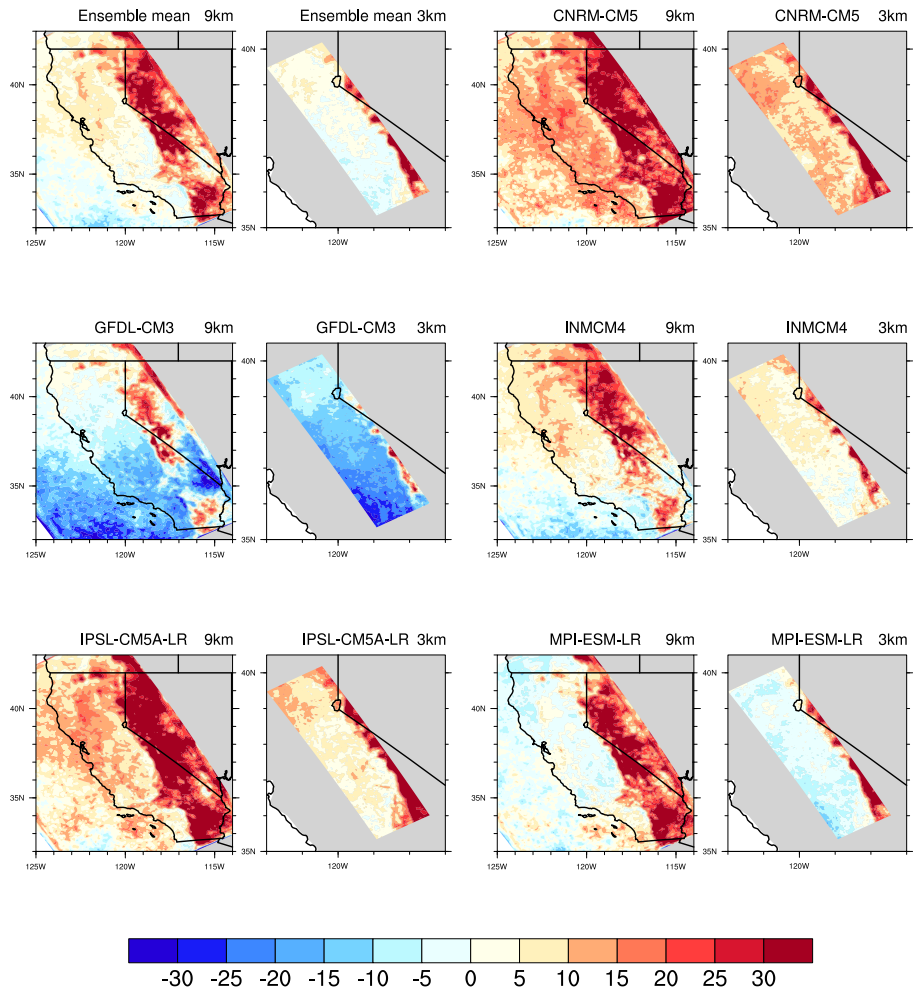


FIG. 10. The relative changes of the rainy days during wet season (NDJFM) from past to future.

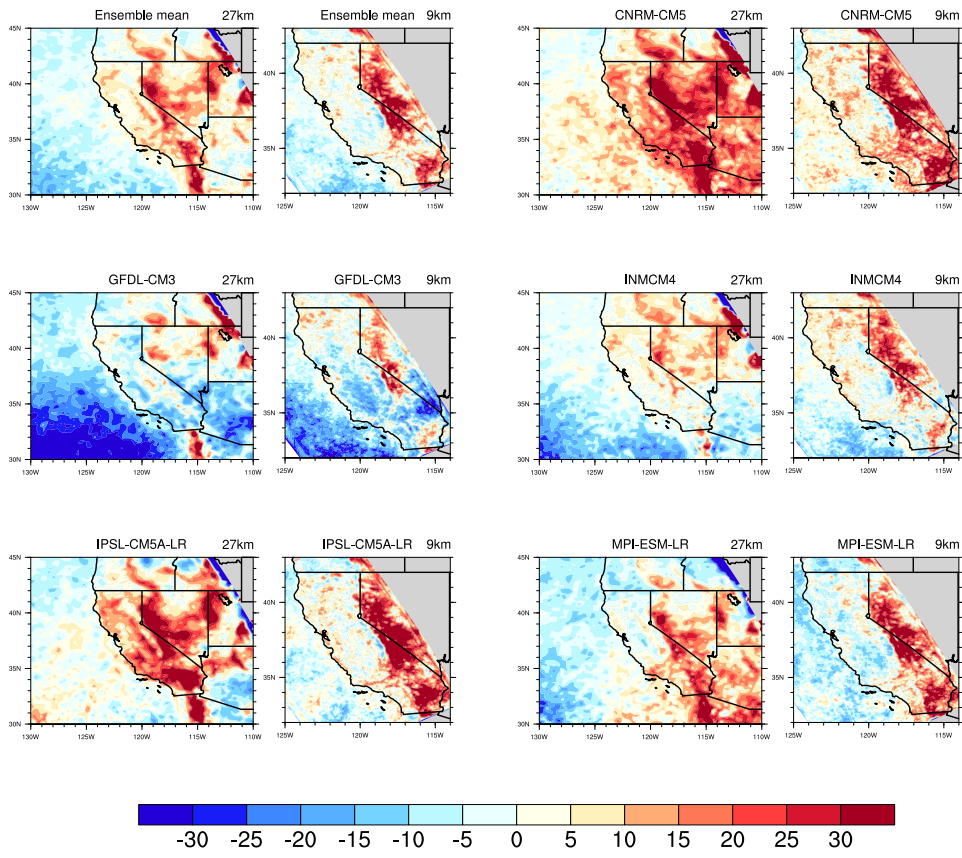


FIG. 11. Similar as Figure 10, but for low-rainy days.

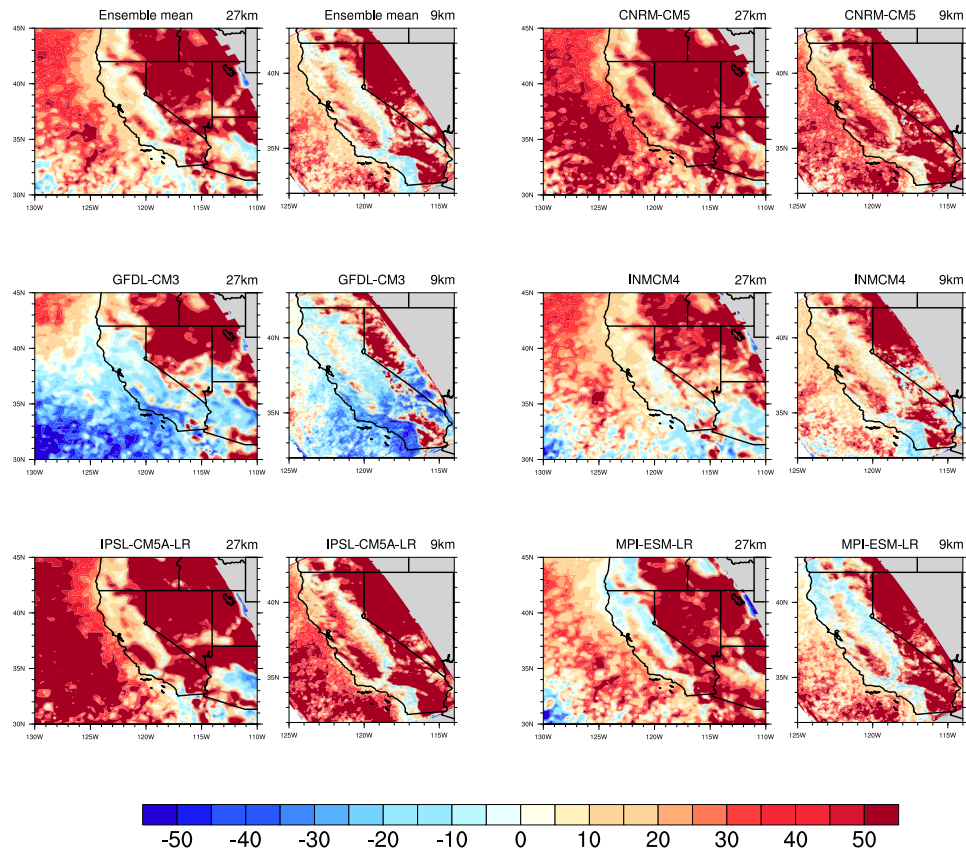


FIG. 12. Similar as Figure 10, but for heavy-rainy days.

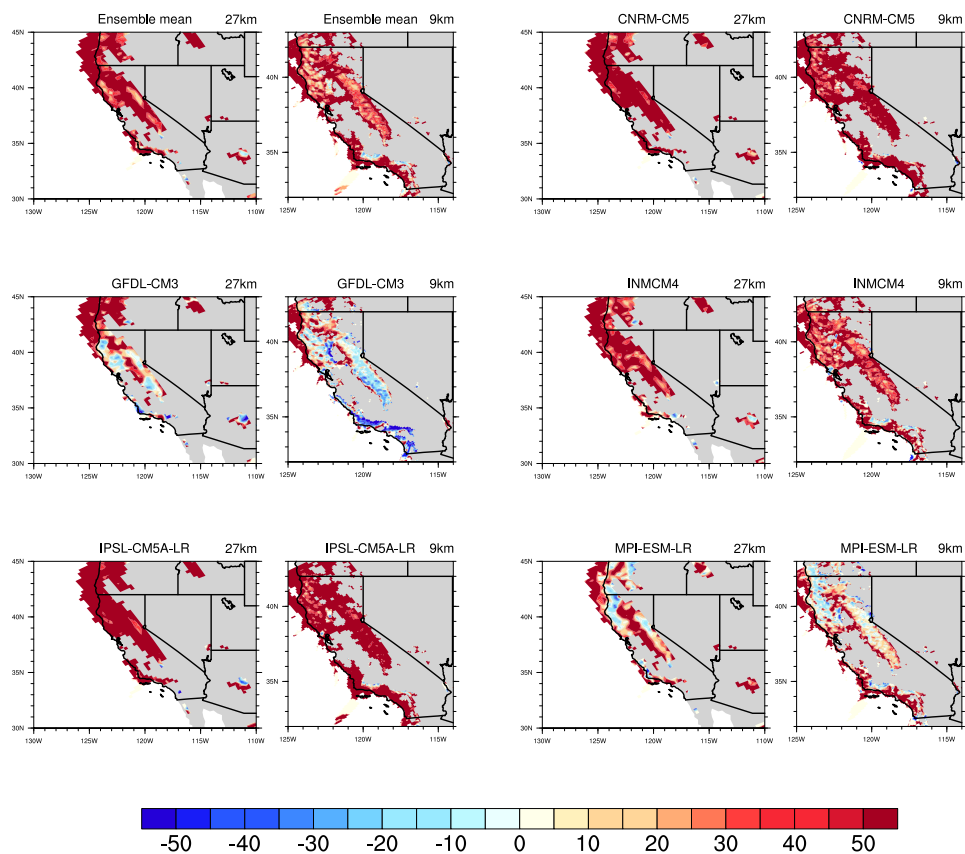


FIG. 13. Similar as Figure 10, but for extremes.

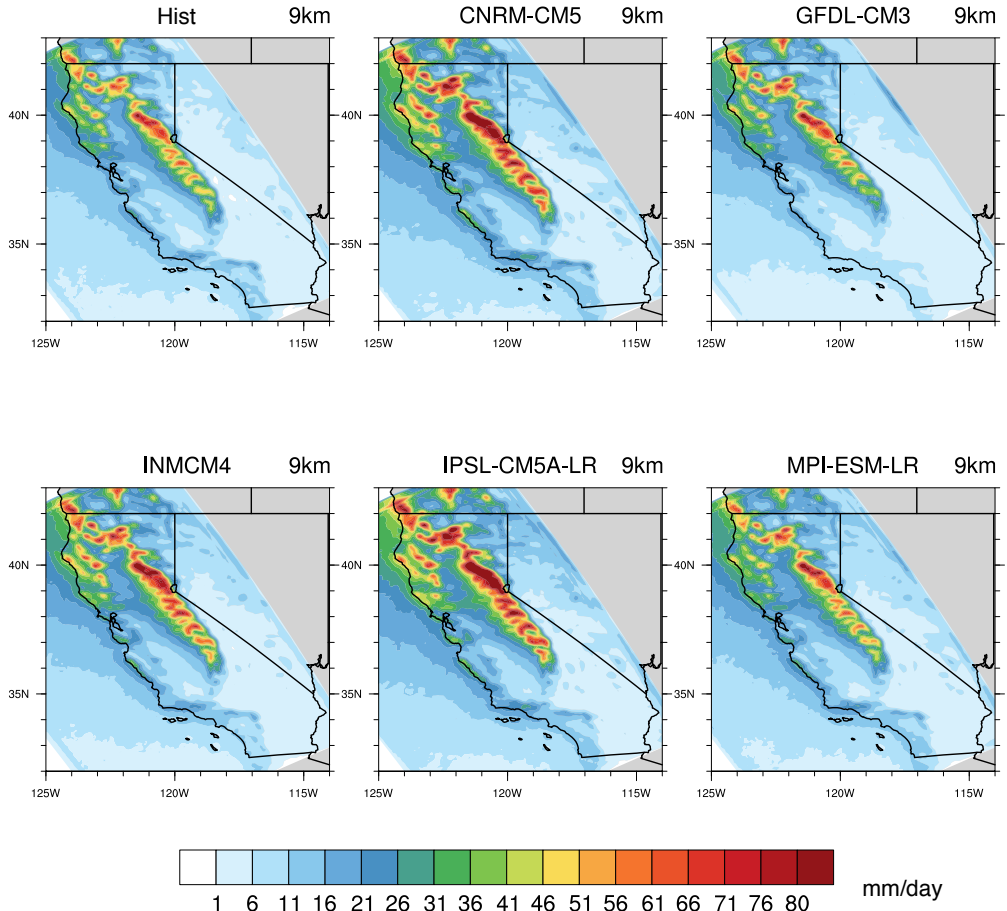
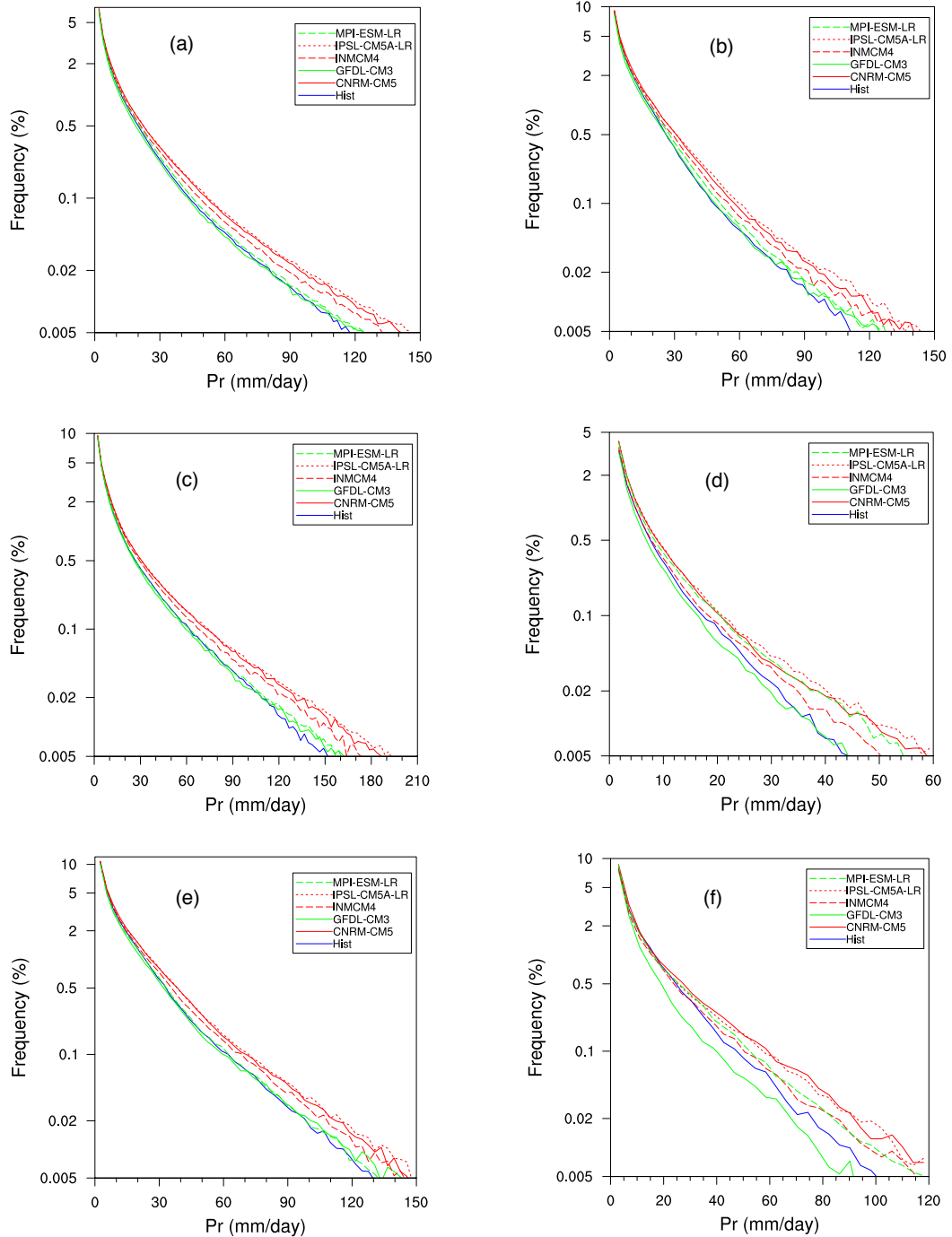
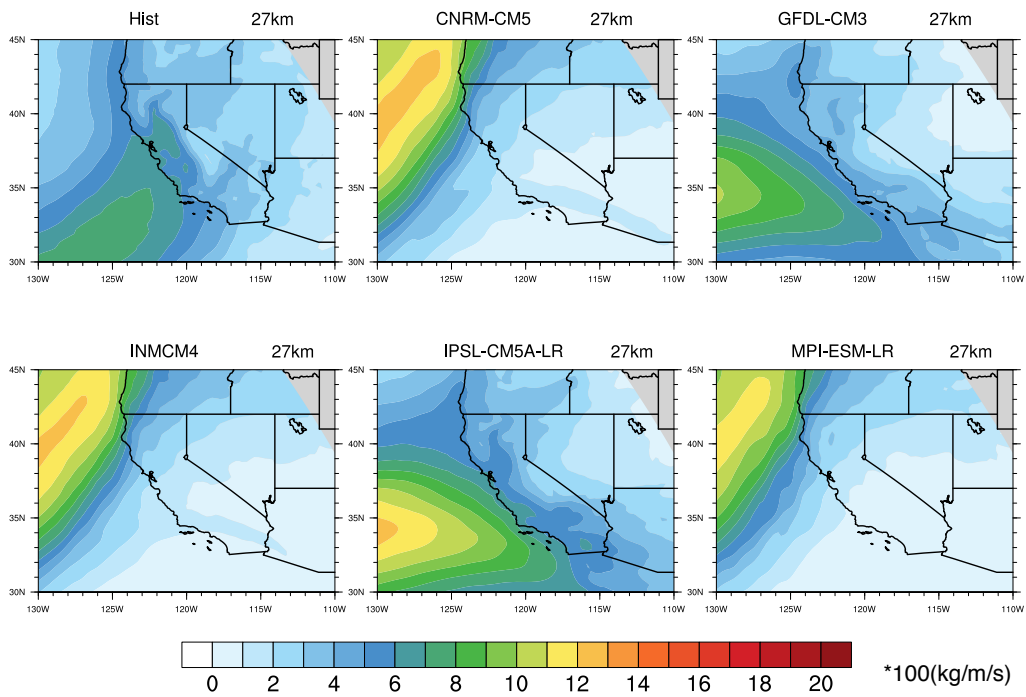


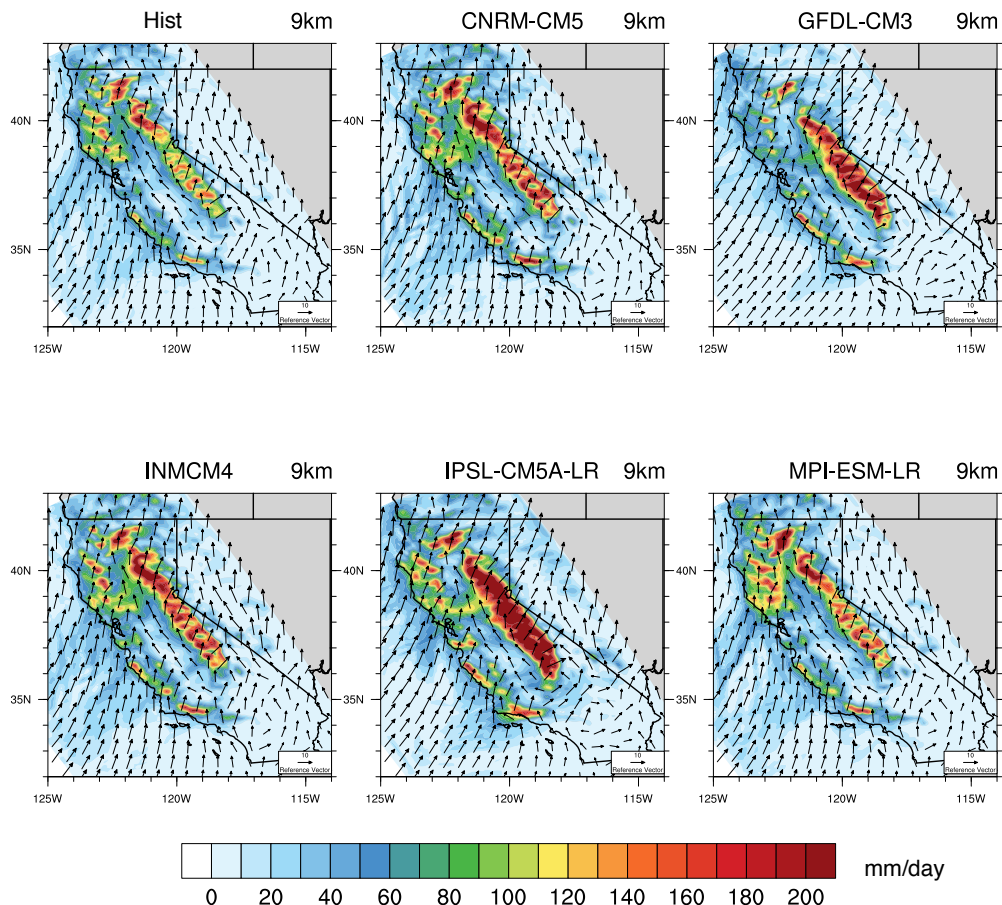
FIG. 14. The 95th quantile (P95) of daily Pr at each grid point for hist and future at 9 km.



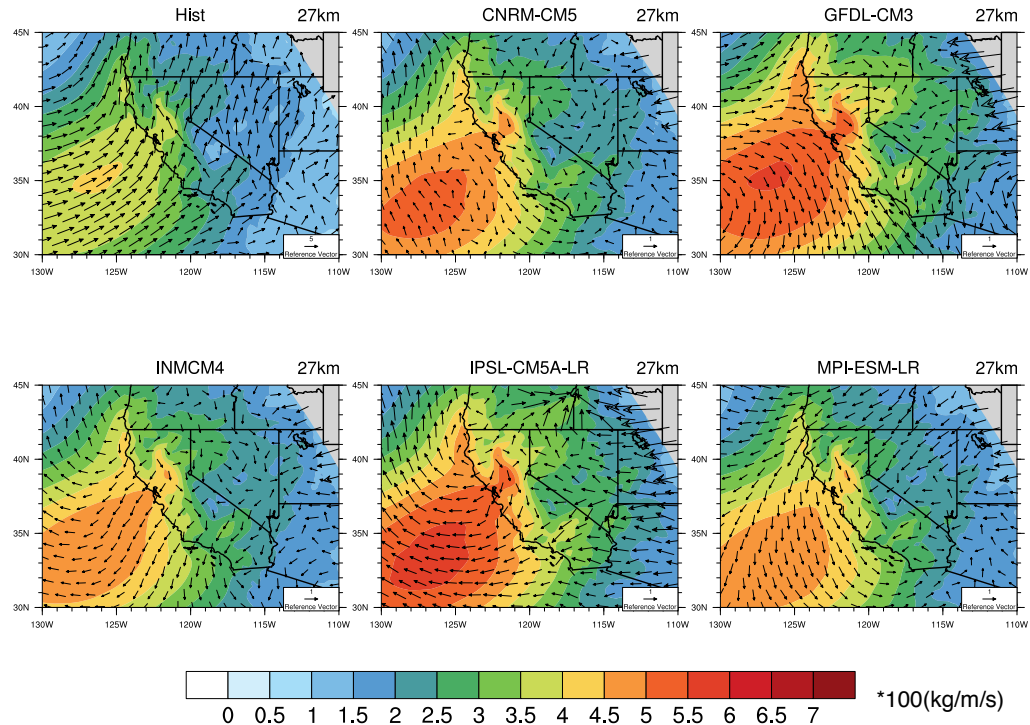
153 FIG. 15. The frequency distribution of daily $Pr (>1\text{mm/day})$ based on all the grid points within different
 154 climate divisions for hist and future at 9 km. Note: (a) California, (b) Central Valley, (c) Mountain region, (d)
 155 Desert area, (e) North coast, (f) South coast.



156 FIG. 16. The integrated water vapor transport (IVT) of the maximum 1 day Pr during the simulation periods
 157 for hist and future at 27 km.



158 FIG. 17. The near-surface wind pattern (at 10 m, unit: m/s) and Pr of the maximum 1 day Pr event for hist
 159 and future at 9 km.



160 FIG. 18. The average IVT and mean wind pattern as the mean Pr over CA exceeds the P95 value for hist and
 161 future at 27 km. Note: Here, the wind patterns for future simulations are the difference between specific future
 162 simulation and historical result.

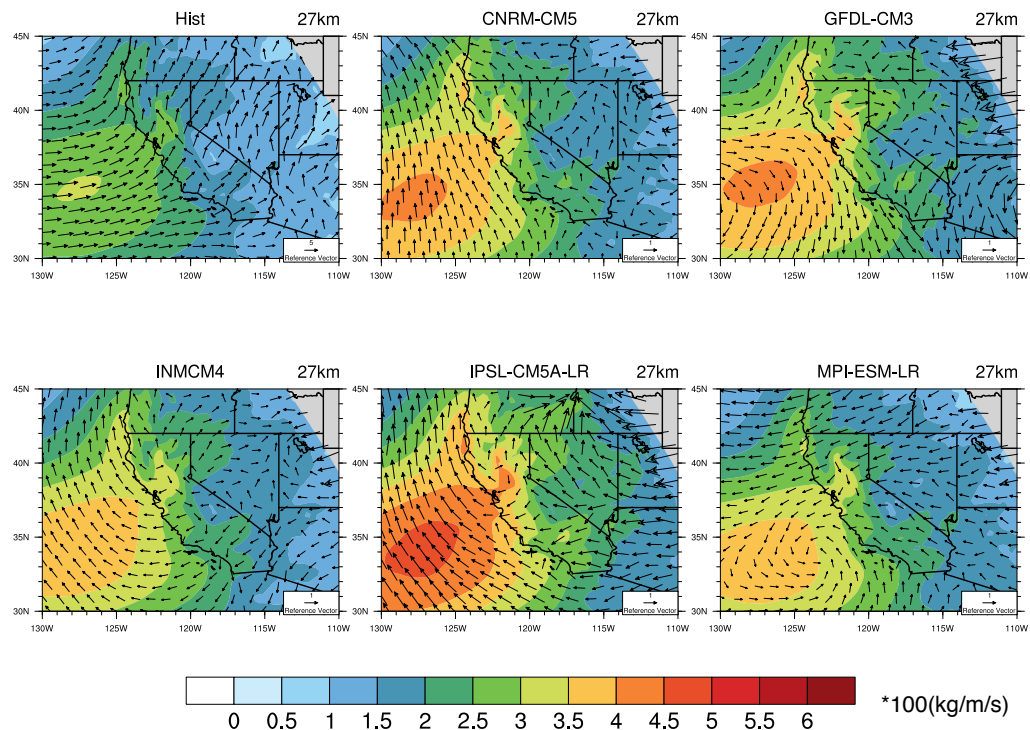


FIG. 19. Similar as Figure 18, but for the case when Pr exceeds the P85 value.